



## MEASURING AIR–WATER INTERFACE AREA IN SUPERCRITICAL OPEN CHANNEL FLOW

HUBERT CHANSON\*

Senior Lecturer in Fluid Mechanics, Hydraulics and Environmental Engineering, Department of Civil Engineering, The University of Queensland, Brisbane QLD 4072, Australia

(First received March 1996; accepted in revised form October 1996)

**Abstract**—In storm waterways and at dam outlets, high-velocity supercritical flows are characterized by substantial air bubble entrainment. The entrainment of fine air bubbles and the strong turbulent mixing contribute both to the air–water transfer of volatile gases (e.g. oxygen, nitrogen, VOC). The paper describes new experimental data obtained in a 25 m long channel with a 4° slope. The analysis of the data provides new information on the air–water flow properties and on the distributions air–water interface area. Although the amount of entrained air is small (i.e. typically  $C_{\text{mean}} < 0.12$ ), the specific air–water interface area can reach over 100 m<sup>2</sup> per unit volume of air and water. The results are compared with an earlier prediction (Chanson, 1994) and confirm the significant contribution of air entrainment to air–water gas transfer in supercritical chute flows. © 1997 Elsevier Science Ltd.

**Key words**—air–water interface area, experimental measurement, open channel flow, air bubble entrainment, gas transfer

### NOMENCLATURE

$a$  = specific interface area (m<sup>-1</sup>) defined as the air–water surface area per unit volume of air and water

$C$  = air concentration defined as the volume of air per unit volume of air and water; it is also called void fraction

$C_{\text{mean}}$  = mean air concentration defined in term of  $Y_{90}$ :  $d = Y_{90}(1 - C_{\text{mean}})$

$ch$  = chord length (m)

$ch_{\text{ab}}$  = air bubble chord length (m)

$(ch_{\text{ab}})_{\text{max}}$  = maximum chord length (m) detected during the scanning time  $t$

$(ch_{\text{ab}})_{\text{NMS}}$  = mean bubble size (m) or the number mean size defined as

$$(ch_{\text{ab}})_{\text{NMS}} = \frac{\sum_{i=1}^{N_{\text{ab}}} n_i (ch_{\text{ab}})_i}{\sum_{i=1}^{N_{\text{ab}}} n_i}$$

$d$  = (1) flow depth (m) measured perpendicular to the flow direction

(2) characteristic water flow depth (m) defined as:

$$d = \int_0^{Y_{90}} (1 - C) dy$$

$d_0$  = flow depth (m) at the channel intake

$Fr$  = Froude number

$g$  = gravity constant:  $g = 9.80 \text{ m/s}^2$  in Brisbane, Australia

$i$  = integer

$N_{\text{ab}}$  = number of air bubbles

$n_i$  = number of air bubbles in interval  $i$

$q_w$  = water discharge per unit width (m<sup>2</sup>/s)

$t$  = (1) time (s)

(2) scanning time (s)

$V$  = velocity (m/s)

$V_{90}$  = characteristic velocity (m/s) where  $C = 0.9$

$W$  = channel width (m)

$x$  = distance (m) along the channel bottom from the channel intake

$Y_{90}$  = characteristic air–water flow depth (m) where  $C = 0.9$

$y$  = distance (m) measured normal to the flow direction

$\delta$  = boundary layer thickness (m)

### Subscripts

air = air flow

o = intake flow conditions

w = water flow

### INTRODUCTION

An important parameter in the assessment of the water quality of rivers and streams is the dissolved oxygen (DO) concentration. In running waters (e.g. streams, rivers), most dissolved oxygen is derived from free-surface aeration (i.e. gas transfer at the free surface). Supercritical open channel flows contribute substantially to the mass transfer process in rivers and streams. They are characterized by strong turbulent mixing and a large amount of air bubble entrainment. Air–water gas transfer across the air bubble interface is predominant as the net surface area of thousands of tiny bubbles can be very important.

Although a large amount of data is available to predict the air–water flow properties of supercritical

\*[Fax: +61 7 3365 4599].

flows (e.g. Wood, 1991; Chanson, 1994), there is little information on the air-water interface area and bubble size distributions within the flow. Wilhelms and Gulliver (1989) and Chanson (1995) discussed the air-water gas transfer process. Gulliver *et al.* (1990) and Chanson (1994) attempted to derive bubble size predictions. However, the accuracy of these methods is still somewhat questionable.

In the paper, new experimental results obtained in a 25 m long flume are presented. Highly sensitive instrumentation (conductivity probe) was used to detect bubbles as small as 0.1 mm. Full details of the results were reported in Chanson and Cummings (1996).

## MATERIALS AND METHODS

### Experimental apparatus

New experiments were conducted in a 25 m long channel with a 4.0° slope located in the Hydraulics-Fluid Mechanics Laboratory of the University of Queensland. The flume was 0.5 m wide and made of planed wooden boards. Water was supplied in a closed-circuit system with an electronically controlled pump, enabling a fine discharge adjustment. The water discharge was measured with a Dall tube flowmeter. Flow to the flume was fed through a smooth convergent nozzle (1.7 m long). The nozzle had a flat bottom, aligned with the flume bottom, two elliptic convergent side-walls and an elliptic convergent roof. The nozzle exit was 30 mm high and 0.5 m wide. The measured contraction ratio was approximately unity: the flow depth at the open-channel intake was 30 mm.

### Instrumentation

Clear-water velocities were measured with a Pitot tube (3.3 mm external diameter). Air-water velocity and air concentration distributions were recorded using a dual-tip conductivity probe. The double-tip conductivity probe was developed at the Hydraulics-Fluid Mechanics Laboratory of the University of Queensland. The probe consists of two identical tips with an internal concentric electrode (of 25 µm diameter) made of platinum and an external stainless steel electrode of 200 µm diameter. The tips are aligned in the flow direction and the distance between tips is 7.42 mm. Both tips are excited by an electronic circuitry (AS25240) which was designed with a response time of less than 10 µs and was calibrated with a square wave generator.

The translation of the probe in the direction normal to the channel bottom was controlled by a fine adjustment travelling mechanism connected to a Mitutoyo digimatic scale unit (ref. no. 572-503). The error on the vertical position of the probe was less than 0.01 mm. The system (probe and travelling mechanism) was mounted on a trolley travelling parallel to the channel bottom (accuracy of about  $\Delta x = 1$  cm).

### Data processing

At each position  $\{x, y\}$  measurements were recorded using the double-tip conductivity probe with a scan rate of 40 kHz per channel for a 5.12 s scan period. The air concentration  $C$  was compared as the probability of encountering air at the leading tip of the probe. The mean air-water velocity  $V$  was computed using a cross-correlation technique. The cross-correlation function between the two tip signals is maximum for the average time taken for an air-water interface to travel from the first tip to the second tip. The velocity is deduced from the time delay between the signals and the tip separation distance.

The chord length\* distributions were also recorded. A dual-tip conductivity probe, used to measure air bubble size characteristics, detects only the bubble chord lengths. If the bubbles are small and spherical, the bubble diameter probability distribution can be deduced from the bubble chord probability distribution (e.g. Clark and Turton, 1988). In the present investigation, the flow field was investigated for void fractions between 0 and 90%. In the region of high concentrations, the structure of the air-water mixture is definitely not bubbly (e.g. Volkart, 1980; Wood, 1991). For these reasons only the "bubble chord length" data are presented.

The chord lengths were calculated at the 50% threshold between air and water, assuming that the bubble velocity equals the local mean air-water velocity.

The air-water interface area was calculated as:

$$a = \frac{4N_{ab}}{Vt}, \quad (1)$$

where  $N_{ab}$  is the number of detected air bubbles† during the scanning period  $t$  and  $V$  is the mean air-water velocity. Equation (1) equals the specific interface area of spherical-bubble mixtures. In high air concentration regions ( $C > 0.3-0.4$ ), the flow structure is more complex and equation (1) is not exactly equal to the specific interface area. Equation (1) simply becomes proportional to the number of air-water interfaces (i.e.  $2N_{ab}$ ) per unit length of air-water mixture (i.e.  $Vt$ ): it still gives some indication of the air-water interface area.

## EXPERIMENTAL RESULTS

Experiments were performed with discharges per unit width between 0.142 and 0.164 m<sup>2</sup> s<sup>-1</sup> with an intake flow depth  $d_0 = 30$  mm. For such discharges, the bottom boundary layer was fully developed at approximately 2.2–2.7 m downstream of the channel intake. The quantity of entrained air (or mean air concentration) was maximum at approximately  $x = 4$  m. Downstream of that location, the mean air content decays gradually as the flow is decelerated (see Table 1 and Fig. 1). Figure 1 shows one set of experimental results for the mean air concentration.

Typical air concentration and velocity distributions are shown in Fig. 2. The measurements were performed on the centreline. They are presented as

Table 1. Summary of air-water flow characteristics for  $q_w = 15$  m<sup>2</sup>/s,  $\alpha = 4$  degrees

$x$ m (1)	$C_{mean}$ (2)	$Y_{90}$ m (3)	$V_{90}$ m/s (4)	$(a)_{max}$ m <sup>-1</sup> (5)	$y/Y_{90}$ (†) (6)	$C$ (†) (7)
4	0.12	0.035	5.03	106	0.91	0.64
12	0.10	0.0446	4.24	71	0.90	0.47
23	0.09	0.0481	3.76	73	0.91	0.48

(†): at the location of maximum specific interface area [i.e.  $a = (a)_{max}$ ].  
( $a$ )<sub>max</sub>: maximum air-water interface area at each cross-section.

\*The bubble chord length is the length of the straight line connecting the two intersections of the air bubble free surface with the leading tip of the probe, as the bubble is transfixied by the probe's sharp edge.

†An air bubble is a "volume" of air detected by the leading tip of the probe between two consecutive air-water interface events. It is an air volume surrounded continuously or not by water interfaces.

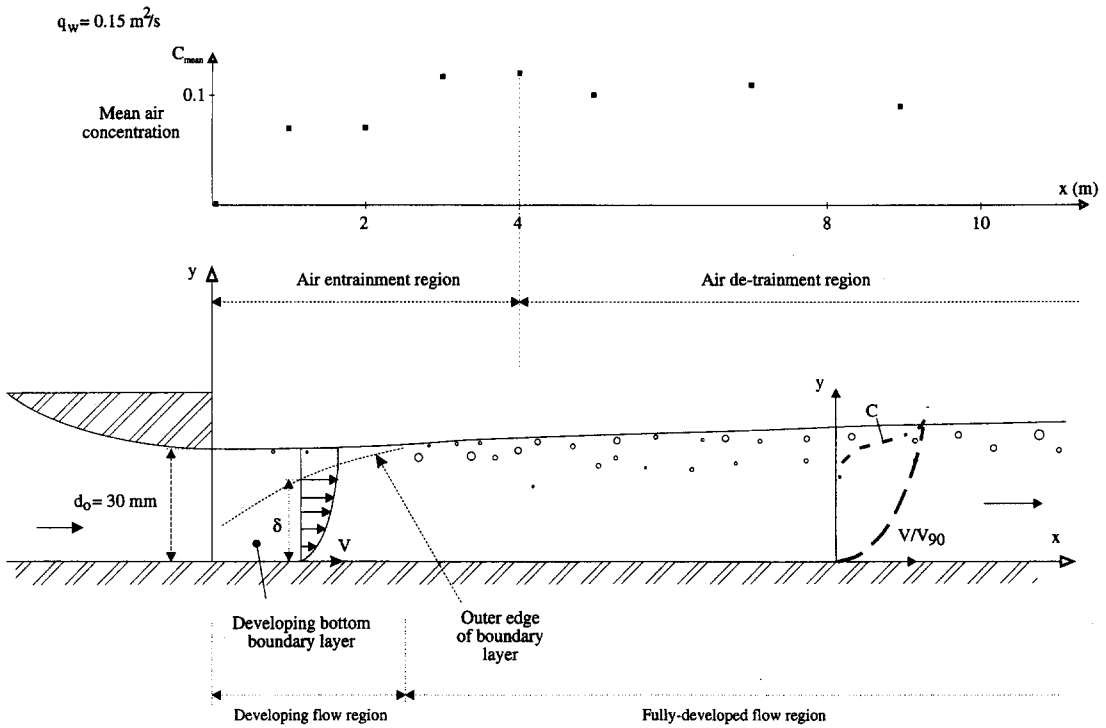


Fig. 1. Sketch of the open channel flow.

$C = f(y/Y_{90})$  and  $V/V_{90} = f(y/Y_{90})$  where  $Y_{90}$  is the distance normal to the bottom where  $C = 0.9$  and  $V_{90}$  is the characteristic velocity at  $Y_{90}$ . The distributions of air content exhibit a smooth shape while the

velocity profiles follow closely a one-sixth power law (Chanson, 1994).

Figure 3 shows bubble chord distributions at various positions along the flume. For each figure, the

$m, Fr_0 = 9.2$

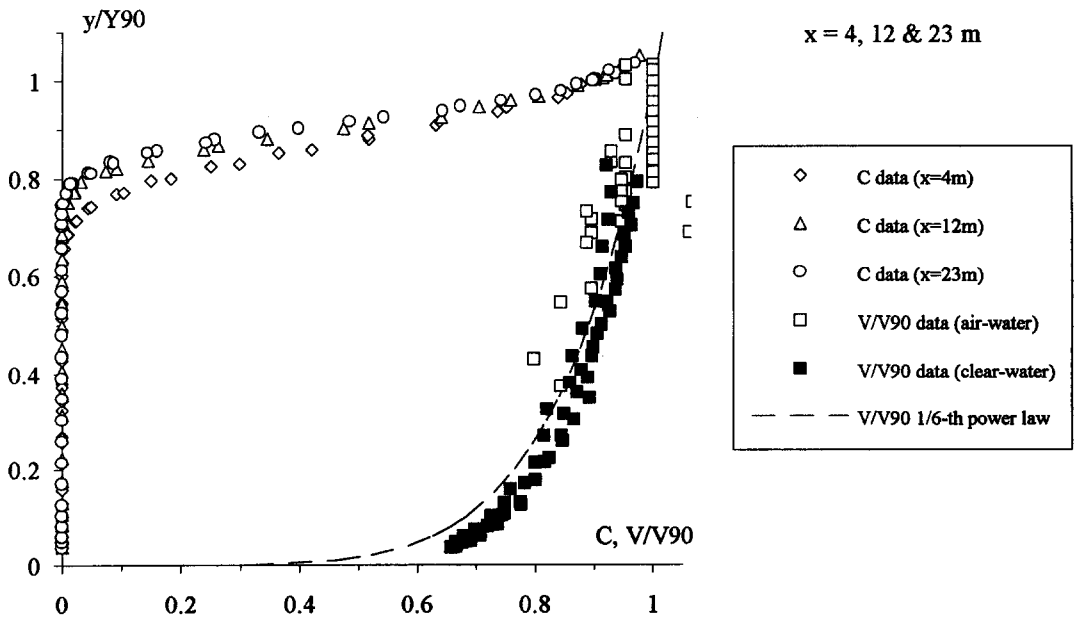


Fig. 2. Air concentration distributions and air-water velocity distributions, with  $q_w = 0.150$  m<sup>2</sup>/s,  $d_0 = 0.03$  m,  $Fr_0 = 9.2$ .

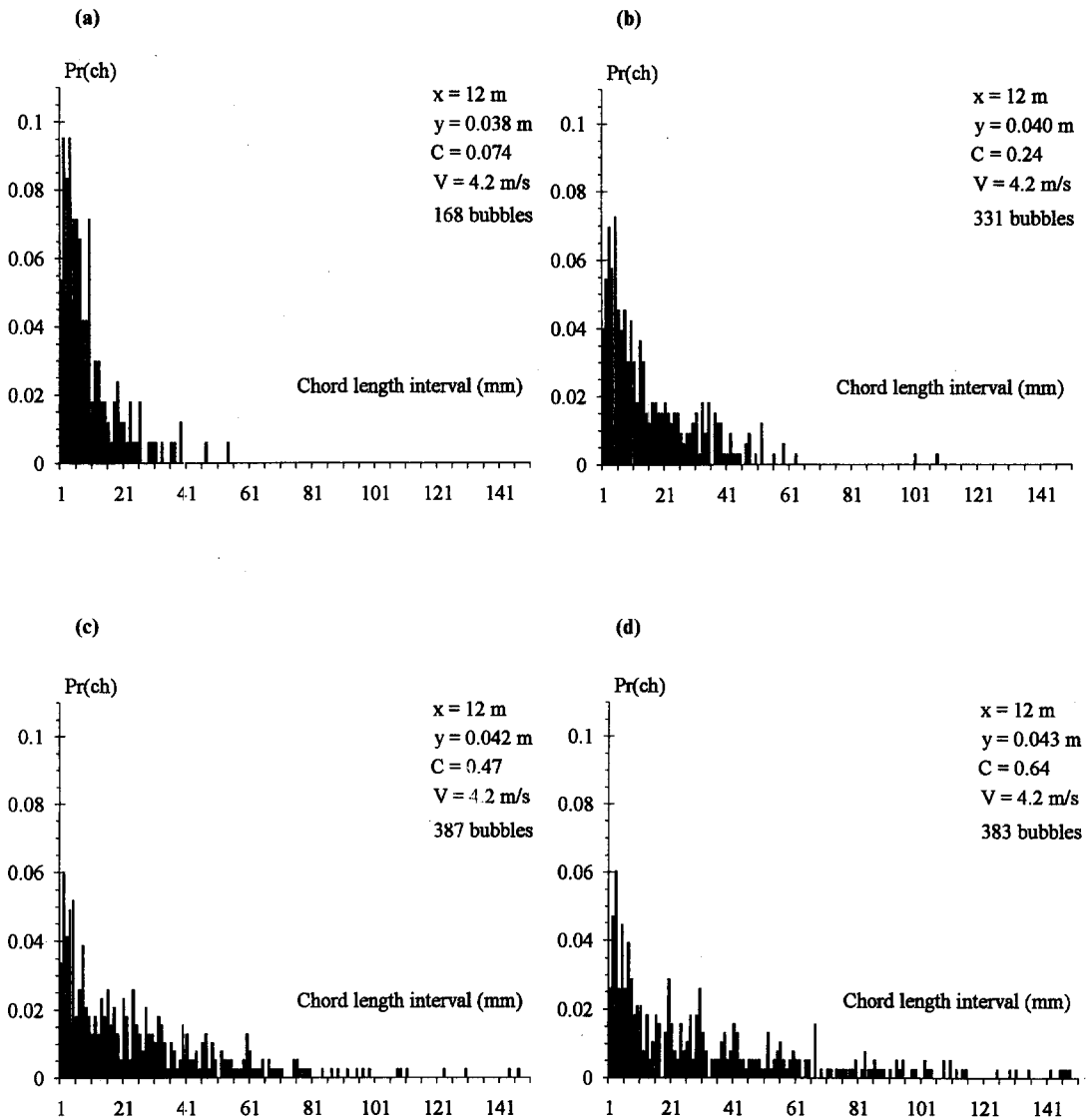


Fig. 3. Chord length distributions at  $x = 12$  m: (a)  $x = 12$  m,  $y = 0.038$  m,  $C = 0.074$ ,  $V = 4.2$  m/s,  $N_{ab} = 168$ ; (b)  $x = 12$  m,  $y = 0.04$  m,  $C = 0.24$ ,  $V = 4.2$  m/s,  $N_{ab} = 331$ ; (c)  $x = 12$  m,  $y = 0.042$  m,  $C = 0.42$ ,  $V = 4.2$  m/s,  $N_{ab} = 387$ ; (d)  $x = 12$  m,  $y = 0.043$  m,  $C = 0.64$ ,  $V = 4.2$  m/s,  $N_{ab} = 383$ .

caption provides the local air-water flow properties ( $C$ ,  $V$ ) and the number of recorded air bubbles  $N_{ab}$  during the scan period ( $t = 5.12$  s). The histogram columns each represent the probability of a bubble chord length in a 1 mm interval. For example, the probability of bubble chord length from 4 to 5 mm is represented by the column labelled 5 mm. In Fig. 3, the broad spectrum of bubble chord lengths at each location  $\{x, y\}$  should be noted. Furthermore, the distributions are skewed with a preponderance of small bubble sizes relative to the mean.

Experimental results of specific air-water interface area are plotted in Fig. 4. The results show that the specific interface area can reach large values (i.e. up to  $106$  m<sup>2</sup> per unit volume of air and water) although

the mean air concentration  $C_{\text{mean}}$  is moderate (i.e.  $C_{\text{mean}} \leq 0.12$ ). Furthermore, the interface area increases with increasing distance from the channel bottom (and increasing air concentration) up to a maximum (Table 1) and then decreases in the upper flow region. Note that the flow properties ( $C, V, a$ ) were investigated for  $C < 0.9$  (i.e.  $y < Y_{90}$ ). For  $y > Y_{90}$ , the air-water flow is primarily a form of fine spray, and the conductivity probe measurements are not accurate.

## DISCUSSION

### Mean and maximum air bubble sizes

The dimensionless distributions of number mean

(4)

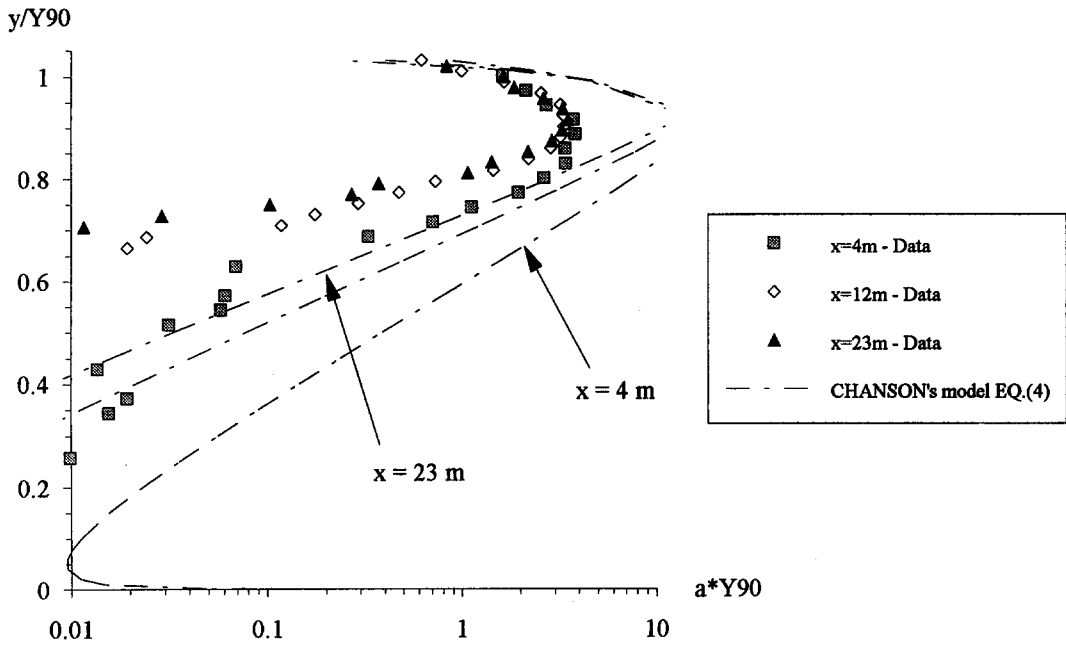


Fig. 4. Dimensionless specific interface area  $aY_{90}$  as a function of  $y/Y_{90}$ ; comparison with equation (4).

chord length size\* (NMS) and maximum chord length size are presented in Fig. 5. Figure 5 shows that both the number mean size and the maximum size increase with increasing distance from the channel bottom and with increasing air content. Note also the rapid increase of bubble size in the high air-content region (i.e.  $C > 0.3-0.4$ ) as illustrated in Fig. 5(a).

For all the experiments, the ratio of the maximum bubble size over the number mean size typically ranges from two to 12. The results are best correlated by:

$$\frac{(ch_{ab})_{max}}{(ch_{ab})_{NMS}} = 1 + 7.14 \left( \frac{y}{Y_{90}} \right)^{2.64}, \quad (2)$$

with a correlation of 0.782.

*Comparison with other results*

The author (Chanson, 1994) developed a crude model to estimate the maximum bubble size in self-aerated flow. Assuming that the bubble size is of the order of magnitude of the mixing length of the

turbulent eddies responsible for bubble break-up, it yields:

$$\frac{(d_{ab})_{max}}{Y_{90}} \sim \sqrt[3]{\frac{72}{(We)_c} \cdot \left( \frac{y}{Y_{90}} \right)^{5/3}}, \quad (3)$$

where  $(We)_c = \rho_w V_{90}^2 Y_{90} / \sigma$ ,  $\rho_w$  is the water density and  $\sigma$  is the surface tension.

Equation (3) is shown in Fig. 5(b). In the low air-content region (i.e.  $C < 0.3-0.4$ ), equation (3) provides some information on the order of magnitude of the mean bubble size, but underestimates the maximum size.

Gulliver *et al.* (1990) re-analysed high-speed photographs of a sectional view of self-aerated flows through a glass side-wall. The photographs were taken by Straub and colleagues (1953, 1956, 1958). The analysis of Straub's photographs suggested that the maximum bubble size (defined such that 95% of the total air volume is encompassed by bubbles of smaller size) was about 2.7 mm, independent of the distance  $y$  from the channel bottom, with most bubble sizes being between 0.7 and 2.7 mm.

The present investigation shows clearly that the range of bubble sizes is broader (Figs 3 and 5). It is a function of the distance from the channel bottom and of the local air concentration. The writer believes that the analysis of Gulliver *et al.* (1990) was based upon bubble size distributions in the side-wall boundary layer which is characterized by higher shear stress and smaller bubble sizes than on the centre-line.

\*The mean bubble size can be defined as the Sauter mean size, volume mean size or number mean size. The number mean size is a better representation of the smaller bubble sizes. It is used here because our interest lies in the air-water interface area and small air bubbles contribute more per unit volume than large bubbles.

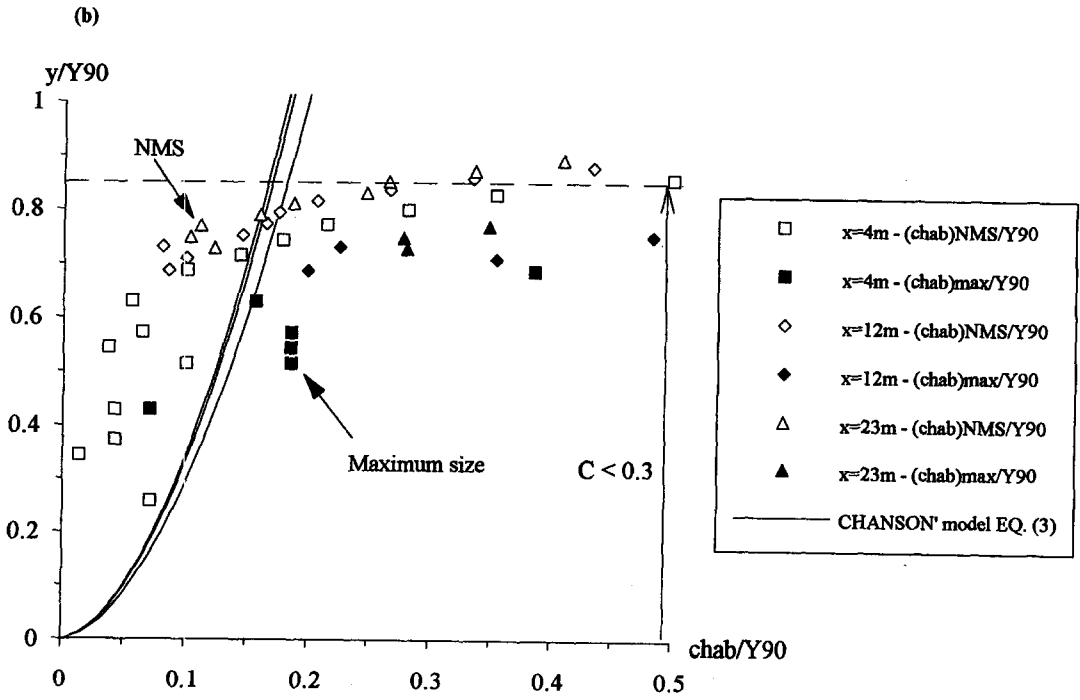
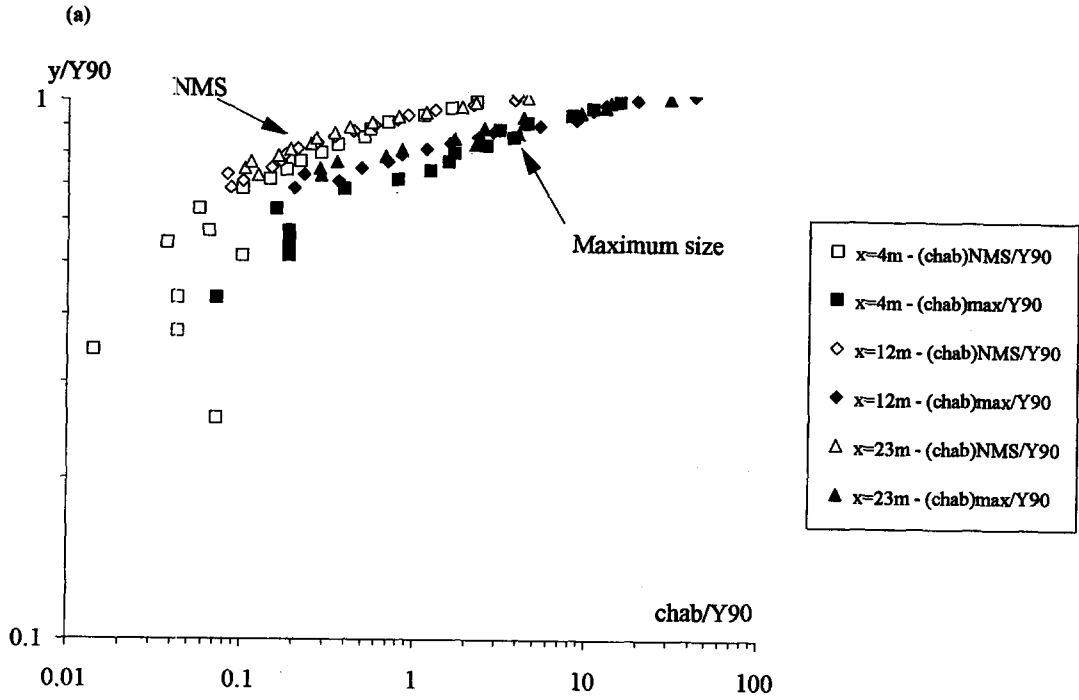


Fig. 5. Dimensionless distributions of number mean chord length size  $(ch_{ab})_{NMS}/Y_{90}$  and maximum chord length size  $(ch_{ab})_{max}/Y_{90}$ : (a) logarithmic presentation; (b) distributions in the low air-content region (i.e.  $C < 0.3-0.4$ ); comparison with equation (5).

### Comparison with an air–water interface area model

The author (Chanson, 1994) developed a rough estimate of the specific air–water interface in self-aerated flows:

$$a = 6 \cdot \frac{C}{(d_{ab})_{\max}} \quad \text{for } C < 0.5 \quad (4a)$$

$$a = 6 \cdot \frac{(1 - C)}{(d_{ab})_{\max}} \quad \text{for } C > 0.5 \quad (4b)$$

where  $(d_{ab})_{\max}$  was computed as in equation (2). Equation (4) is reported in Fig. 4. Although equation (4) is a very crude approximation, it is interesting to note the similarity of shape between the data and equation (4) as well as the same order of magnitude between the data and calculations.

The experimental results suggest that self-aerated flows down open channels can entrain a substantial amount of air bubbles, and the cumulative air–water interface of the bubbles is large. The present investigation shows that previous air–water interface area calculations [i.e. equations (3) and (4)] are not accurate. However, they give the same qualitative trends for the distribution of mean bubble size and specific interface area as the experimental results. The calculations also provide quantitative results of the same order of magnitude as the data.

Altogether, the present study suggests that previous calculations of air–water interface area and air–water gas transfer (Chanson, 1994, 1995) are some form of reasonable approximation.

### CONCLUSION

New measurements of air–water flow in open channels provide new information on the air–water flow properties. An accurate measurement technique based upon conductivity probes gives details of bubble chord lengths and chord length profiles.

The bubble chord length distributions exhibit very broad ranges, suggesting the entrainment of both individual air bubbles and bubble clusters, air pockets and possibly the existence of emulsified flow (i.e. foam).

The analysis of the velocity and chord length data enables us to estimate the local interface area. Typical

results are presented in Fig. 4. The air–water interface area can reach very large values (i.e. more than 100 m<sup>2</sup> per unit volume) despite the limited amount of entrained air (i.e.  $C_{\text{mean}} < 0.12$ ). Such results emphasize the contribution of air bubble entrainment to the air–water gas transfer process in open channel flows.

It is worth mentioning that the present analysis is based upon experiments performed in a large channel with high-velocity flows: i.e. a 25 m long channel ( $W = 0.5$  m) with upstream Froude numbers ranging from 8.7 to 10.1. Such a geometry should preclude any scale effects as the size of the experiment is close to most full-scale applications.

*Acknowledgements*—This research project is supported by the Australian Research Council (ref. no. A89331591). The author acknowledges the assistance of Dr P. D. Cummings.

### REFERENCES

- Chanson H. (1994) Air–water interface area in self-aerated flow. *Water Res. IAWPRC* **28**(4), 923–929.
- Chanson H. (1995) Predicting oxygen content downstream of weirs, spillways and waterways. *Proc. Inst. Civil Eng., Water, Maritime and Energy* **112**, 20–30.
- Chanson H. and Cummings P. D. (1996) Air–water interface area in supercritical flows down small-slope chutes. Research Report No. CE151, Department of Civil Engineering, University of Queensland.
- Clark N. N. and Turton R. (1988) Chord length distributions related to bubble size distributions in multiphase flows. *Int. J. Multiphase Flow* **14**(4), 413–424.
- Straub L. G. and Anderson A. G. (1958) Experiments on self-aerated flow in open channels. *J. Hyd. Div. Proc. ASCE* **84** (HY7) paper 1890, 1890-1–1890-35.
- Straub L. G. and Lamb O. P. (1953) Experimental studies of air entrainment in open-channel flows, pp. 425–437. In *Proceedings of the 5th IAHR Congress, IAHR-ASCE*, Minneapolis, U.S.A.
- Straub L. G. and Lamb O. P. (1956) Studies of air entrainment in open-channel flows. *Trans. ASCE* **121**, 30–44.
- Volkart P. (1980) The mechanism of air bubble entrainment in self-aerated flow. *Int. J. Multiphase Flow* **6**, 411–423.
- Wilhelms S. C. and Gulliver J. S. (1989) Self-aerating spillway flow, pp. 481–533. In *Proceedings of the National Conference on Hydraulic Engineering* (Edited by Ports M. A.), ASCE, New Orleans.
- Wood I. R. (1991) Air entrainment in free surface flows. *IAHR Hydraulic Structures Design Manual No. 4, Hydraulic Design Considerations*. Balkema Publ., Rotterdam.